AFRL-AFOSR-JP-TR-2016-0100

Photonic Nanoparticle-Doped Architectures for Enhanced Solar-to-Fuel Photocatalytic Conversion - 154060

Tai-Chou Lee
NATIONAL CENTRAL UNIVERSITY

12/09/2016
Final Report

Air Force Research Laboratory
AF Office Of Scientific Research (AFOSR)/ IOA
Arlington, Virginia 22203
Air Force Materiel Command

REPORT DOCUMENTATION PAGE

Form Approved
OMB No. 0704-0188

1. REPORT DATE *(DD-MM-YYYY)*	2. REPORT TYPE	3. DATES COVERED *(From - To)*
09-12-2016	Final	10 Sep 2015 to 09 Sep 2016

4. TITLE AND SUBTITLE
Photonic Nanoparticle-Doped Architectures for Enhanced Solar-to-Fuel Photocatalytic Conversion - 154060

5a. CONTRACT NUMBER

5b. GRANT NUMBER
FA2386-15-1-4101

5c. PROGRAM ELEMENT NUMBER
61102F

6. AUTHOR(S)
Tai-Chou Lee, Randall Lee

5d. PROJECT NUMBER

5e. TASK NUMBER

5f. WORK UNIT NUMBER

7. PERFORMING ORGANIZATION NAME(S) AND ADDRESS(ES)
NATIONAL CENTRAL UNIVERSITY
300, JHONGDA RD.
CHUNGLI CITY, 32001 TW

8. PERFORMING ORGANIZATION REPORT NUMBER

9. SPONSORING/MONITORING AGENCY NAME(S) AND ADDRESS(ES)
AOARD
UNIT 45002
APO AP 96338-5002

10. SPONSOR/MONITOR'S ACRONYM(S)
AFRL/AFOSR IOA

11. SPONSOR/MONITOR'S REPORT NUMBER(S)
AFRL-AFOSR-JP-TR-2016-0100

12. DISTRIBUTION/AVAILABILITY STATEMENT
A DISTRIBUTION UNLIMITED: PB Public Release

13. SUPPLEMENTARY NOTES

14. ABSTRACT
This research focused on synthesis of unique plasmonic nanoparticles, preparation of core-shell particles to enhance generation of hydrogen via the photocatalytic splitting of water, and mechanistic studies of charge transfer of such core-shell particles. Particular emphasis centered on synthesis and study of hollow gold-silver nanoshells (GS-NSs) having tunable localized surface plasmon resonances (LSPRs). We prepared three sizes of GS-NSs with LSPR maxima centered at 500, 700, and 900 nm. Subsequently, we coated the GS-NSs with a shell of silica (SiO2) having two different thicknesses, 17 nm and 42 nm. The generated GS-NSs (uncoated and SiO2-coated) were then coated with the photocatalyst, which in our case is the semiconductor zinc indium sulfide (ZnIn2S4; ZIS). After evaluating the photocatalytic water splitting activities, we found that GS-NS(700 nm)@SiO2(17 nm)@ZIS has the most enhancement factor (2.6) compared to that of ZIS without GS-NSs. The lifetime of photo-generated electrons in the conduction band of the photocatalyst was observed using time-resolved photoluminescence (TRPL). To prepare a better coverage of the ZIS coating on the SiO2 surface, 3-mercaptopropyltrimethoxysilane (MPS) was used modify the SiO2 surface. The ZIS shell was then grown on the SiO2 surface to afford composite particles having a smooth morphology. We found that decreasing the concentration of photocatalyst precursor and increasing the content of SiO2 leads to a better coverage of the ZIS shell. We are also exploring the use of nanoshells coated with tin oxide (SnO2) rather than silica (SiO2) and coating the GS-NSs with zinc- and antimony-doped SnO2. Furthermore, we developed new routes for the preparation of silver, platinum, and palladium seed nanoparticles and demonstrated their use in the facile synthesis of Ag, Pt, Pd, and Pt/Ag nanoshells. Separate studies explore the

15. SUBJECT TERMS
Hydrogen Generation, Metal Nanoshells, Photocatalysis

16. SECURITY CLASSIFICATION OF:			17. LIMITATION OF ABSTRACT	18. NUMBER OF PAGES	19a. NAME OF RESPONSIBLE PERSON
a. REPORT	b. ABSTRACT	c. THIS PAGE			CASTER, KENNETH
Unclassified	Unclassified	Unclassified	SAR	22	19b. TELEPHONE NUMBER *(Include area code)* 315-229-3326

Final Report for AOARD Grant 15IOA101
"Photonic Nanoparticle-Doped Architectures for Enhancing Solar-to-Fuel Photocatalytic Conversion"
Date: Dec. 2, 2016

PI and Co-PI information:
PI: Tai-Chou Lee; taichoulee@ncu.edu.tw; National Central University; Department of Chemical and Materials Engineering; 300 Jhongda Road, Jhongli District, Taoyuan County, Taiwan; +886-3-4227151#34211

Co-PI: T. Randall Lee, trlee@uh.edu; University of Houston; Department of Chemistry; 4800 Calhoun Road, Houston, Texas 77204, United States; +1-713-7432724

Period of Performance: Sep./10/2015 – Sep./9/2016

Abstract

Research funded by this award focused on the synthesis of unique plasmonic nanoparticles, preparation of core-shell particles to enhance the generation of hydrogen via the photocatalytic splitting of water, and mechanistic studies of the charge transfer of such core-shell particles. A particular emphasis centered on the synthesis and study of hollow gold-silver nanoshells (GS-NSs) having tunable localized surface plasmon resonances (LSPRs). We prepared three sizes of GS-NSs with LSPR maxima centered at 500, 700, and 900 nm. Subsequently, we coated the GS-NSs with a shell of silica (SiO_2) having two different thicknesses, 17 nm and 42 nm. The generated GS-NSs (uncoated and SiO_2-coated) were then coated with the photocatalyst, which in our case is the semiconductor zinc indium sulfide ($ZnIn_2S_4$; ZIS). After evaluating the photocatalytic water splitting activities, we found that GS-NS(700 nm)@SiO_2(17 nm)@ZIS has the most enhancement factor (2.6) compared to that of ZIS without GS-NSs. The lifetime of photo-generated electrons in the conduction band of the photocatalyst was observed using time-resolved photoluminescence (TRPL). The increase of electron density can be retrieved by comparing the charge-carrier dynamics with and without the excitation of GS-NSs. To prepare a better coverage of the ZIS coating on the SiO_2 surface, 3-mercaptopropyltrimethoxysilane (MPS) was used modify the SiO_2 surface. The ZIS shell was then grown on the SiO_2 surface to afford composite particles having a smooth morphology. We found that decreasing the concentration of photocatalyst precursor and increasing the content of SiO_2 leads to a better coverage of the ZIS shell. We are also exploring the use of nanoshells coated with tin oxide (SnO_2) rather than silica (SiO_2) and coating the GS-NSs with zinc- and antimony-doped SnO_2. Furthermore, we developed new routes for the preparation of silver, platinum, and palladium seed nanoparticles and demonstrated their use in the facile synthesis of Ag, Pt, Pd, and Pt/Ag nanoshells. Separate studies are exploring the use of photonic iron oxide (Fe_3O_4) nanoparticles as co-catalysts in photocatalytic water splitting. Our new synthetic procedures pave the way to generate complex composite structures having controlled nanoscale composition for optimizing solar hydrogen production.

Introduction

This fundamental research effort targets the synthesis and characterization of unprecedented photonic nanoparticle structures and the fabrication and study of the corresponding nanoparticle-based catalysts for solar-to-hydrogen conversion. The intense localized surface plasmon resonance (LSPR) can generate a locally enhanced electric field in the proximity of the metal NPs,[1-4] and this LSPR-induced electric field can promote the photoexcitation of chromophores near metal NPs. Further, a non-conducting SiO_2 shell coated onto Au NPs prevents direct electron transfer between the NPs and the contacting semiconductor material. With nanoshells, the absorption of light is accompanied by the conversion of photon energy to heat and the transfer of heat from the nanoshells to the surroundings. For nanoshells encapsulated within an appropriate matrix, the LSPR can generate two forms of interactions, motivating reactions within the matrix. The exploration and development of these unique nanoparticles and composite catalysts will provide enhanced power conversion efficiencies for solar cells, which will lead to efficient fuel-cell systems and self- powered structures with integrated energy harvesting/storage capabilities.

We prepared samples of these nanoparticles with LSPRs at systematically varying extinction maxima across the visible and into the near infrared (NIR) using modifications of the procedures outlined in a previous report from our research team.[5] Our hypothesis rested on the concept that, when combined with a suitable photocatalyst, the energy absorbed/scattered by the nanoshells would be redistributed to the photocatalyst through various dissipative mechanisms. We prepared three sizes of GS-NSs with LSPR maxima centered at 500, 700, and 900 nm. Subsequently, we coated the GS-NSs with a shell of silica (SiO_2) having two different thicknesses, 17 nm and 42 nm, and evaluated these coated nanoshells to those having no coating. The generated GS-NSs (uncoated and SiO_2-coated) were then coated with the photocatalyst, which in our case is the semiconductor zinc indium sulfide ($ZnIn_2S_4$; ZIS). We evaluated the photocatalytic water splitting activities of these composites and compared the activities to that of undoped ZIS samples. These systematic studies, the results of which are now published,[1] explored ten different types of particles (i.e., ZIS nanocomposites doped with three different GS-NSs that were either uncoated or coated with silica shells having selected thicknesses). The results indicate that doping ZIS photocatalysts with GS-NSs enhances the rate of hydrogen production due to interaction between the LSPR of the plasmonic metal core and the semiconductor shell. Specifically, direct contact between the GS-NS core and ZIS shell (i.e., doping with uncoated GS-NSs) led to enhanced photocatalytic activity compared to ZIS alone.

In our previous work, we developed a microwave-assisted hydrothermal method to generate ZIS shell onto the GS-NS surfaces. However, the coverage and thickness of ZIS on GS-NS were not precisely controlled. In this work, part of the efforts focused on preparing SiO_2 core-ZIS shell nanoparticles with controlled thickness of ZIS shells, to completely utilize the photocatalyst, and optimize the solar hydrogen production. In addition to the preparation of GS-NS@SiO_2 particles, we are also exploring the GS-NS coated with tin oxide (SnO_2) and doped SnO_2. Nanoshells with other architectures, such as Ag, Pt, and Pd nanoshells, Ag-free Au nanocage, and high crystalline Fe_3O_4 were also synthesized. These unique plasmonic nanoparticles will further be tested as the integral part of core-shell particles for solar-to-fuel photocatalytic conversion.

Experiment

Preparation of SiO_2-Coated hollow GS-NSs.

The SiO_2-coated hollow GS-NSs were generated using a modified Stöber method.[6] In this procedure, 10 mL of a solution containing hollow gold nanoshells (GS-NSs)[5] was diluted to 20 mL and then mixed with ammonium hydroxide (2 mL) and ethanol (45 mL). Under vigorous stirring, 25−100 μL of TEOS was added to the solution, depending on the desired thickness of the SiO_2 shells. The mixture was then further stirred overnight at rt to allow the hollow GSNSs to be encapsulated fully by the SiO_2 shells. The resulting solution was centrifuged at 6000 rpm for 20 min and the supernatant decanted, and the nanoshells were redispersed in ethanol. This procedure was repeated four times. Finally, the isolated composite nanoparticles were redispersed into 10 mL of ethanol for characterization and application.

Preparation of GS-NS@SiO_2@ZIS composite structures.

In preparing undoped ZIS particles, zinc nitrate hexahydrate (0.3 mmol), indium(III) nitrate hydrate (0.6 mmol), and thioacetamide (2.4 mmol) were dissolved in 15 mL of deionized (DI) water under vigorous stirring for 20 min. The solution was then poured into a 30-mL quartz vessel. The hydrothermal reaction took place in a microwave reactor (Monowave 300, Anton Paar) at 120 °C for 10 min. The precipitates were collected and centrifuged at 8000 rpm for 5 min. The resulting particles were rinsed thoroughly with DI water several times and then dried in an oven at 80 °C for 12 h. For the synthesis of GS-NS@SiO_2@ZIS particles, a 250-μL aliquot of a nanoshell solution was first dried, and the particles were then redispersed in 15 mL of DI water using ultrasonic vibration. Zinc nitrate hexahydrate (0.3 mmol), indium(III) nitrate hydrate (0.6 mmol), and thioacetamide (2.4 mmol) were dissolved under vigorous stirring. The reaction was then carried out in a microwave oven at 120 °C for 10 min. The as-prepared GS-NS@SiO_2@ZIS particles were collected by centrifugation and washed with DI water several times. Finally, the composite particles were placed in an oven at 80 °C for 12 h to remove excess water. The details of synthesis of GS-NSs and GS-NS@SiO_2 nanoparticles can be found in our publication.[1]

Preparation of SiO_2 and surface modification for subsequent coating with ZIS

The SiO_2 NPs were generated using a modified Stöber method.[6] In this procedure, 30 mL of ethanol was mixed with 2.4 mL ammonium hydroxide in round-bottomed flask and stirred for 5 min. Tetraethylorthosilicate (TEOS; 1.24 mL) was then added into the flask and stirred overnight. The resulting solution was centrifuged at 6000 rpm for 20 min. The synthesized SiO_2 powders were dried in an oven at 80 °C for 12 h to remove excess solution. For modification of the SiO_2 surface, 3-mercaptopropyltrimethoxysilane (MPS) was used. Specifically, 30 mL of ethanol and 2.4 mL of ammonia were mixed and stirred for 5 min. SiO_2 particles (0.20 g) were added and ultrasonicated to generate a uniform dispersion. MPS (100 μL) was then added and stirred overnight. The particles were dried in an oven at 80 °C for 12 h to remove water. Finally, the level of ZIS precursor concentrations and solid content of SiO_2 were varied to achieve optimum coverage on SiO_2.

Preparation of SiO_2@MPS@ZIS

Two solutions were prepared to synthesize ZIS shell on SiO_2@MPS. Solution A was the mixture of 0.09 g zinc nitrate, 0.18 g indium(III) nitrate, dissolved into 50 mL deionized water. Solution B was 0.18 g thioacetamide dissolved into 50 mL deionized water. The preparation of SiO_2@MPS@ZIS was the following. 0.1 g of SiO_2@MPS powder was dispersed in 5 mL deionized water. Solution A (5 mL) was added into SiO_2@MPS aqueous solution. The mixture was then sonicated for 2 h. Solution B (5 mL) was added and stirred for 5 min. Finally, the reaction was then carried out in a microwave oven at 120 °C for 10 min. The SiO_2@MPS@ZIS particles were collected by centrifugation and washed with DI water several times. Finally, the composite particles were placed in an oven at 80 °C for 12 h to remove excess water.

Preparation of Ag@Au@SnO_2

The dried powders of GS-NSs were added into a 50 mL flask with 3 mL of ethanol followed by the addition of 0.2 mL of 0.2 M urea, 0.4 mL of 0.08 M of sodium stannate trihydrate and 50 μL of 0.1 M sodium hydroxide. After stirring at rt for 1 h, the temperature was increased to 135 °C, and the mixture was stirred for 1 h. The as-prepared Ag@Au@SnO_2 particles were collected by centrifugation at 6000 rpm for 15 min and washed with ethanol several times.

Preparation of THPC silver, platinum, and palladium nanoparticles[7]

For the silver nanoparticles prepared in a tetrakis(hydroxymethyl)phosphonium chloride (THPC) solution (THPC-AgNPs), an aqueous solution of sodium hydroxide (0.5 mL, 0.024 g, 0.6 mmol), THPC (12 mL of 80% THPC in 1 mL of water), and 45 mL of Milli-Q water were added to a 100 mL round-bottomed flask and vigorously stirred for 5 min. An aliquot (2 mL, 0.01 g, 0.06 mmol) of aqueous $AgNO_3$ was then added quickly to the mixture. The color of the solution immediately changed from colorless to dark brown-yellow. Vigorous stirring was continued for 10 min. Separately, the palladium nanoparticles generated in a THPC solution (THPC-PdNPs) were prepared in analogous fashion, affording a brown solution. For the procedure, a solution of sodium hydroxide (0.5 mL, 0.02 g, 0.5 mmol), and 1 mL of a THPC solution (12 mL of THPC in 1 mL of water), were vigorously stirred for 5 min in a 100 mL round-bottomed flask containing 45 mL of Milli-Q water. After the allotted time, Na_2PdCl_4 solution (3 mL, 0.02 g, 0.06 mmol) was quickly added to the mixture and stirred for 10 min. Platinum nanoparticles produced from a THPC solution (THPC-PtNPs) were prepared using a slightly different procedure that involved heating 45 mL of water to 90 ℃ in a round-bottomed flask, and then adding a sodium hydroxide solution (0.5 mL, 0.024 g, 0.6 mmol), and subsequently THPC (12 mL of 80% THPC in 1 mL of water). The solution was vigorously stirred for 1 min, and then 3.0 mL of K_2PtCl_4 was added quickly. The solution was vigorously stirred for 10 min and then cooled to room temperature. During the first 10 min of the cool down, the solution turned dark brown in color. Each of the THPC-mNP seed solutions was used as described in the next paragraph.

Preparation of amine-functionalized silica nanoparticles[7]

Large silica core particles were prepared using the well-known Stöber method.[6] Briefly, NH_4OH (1.0 mL) was added to a mixture of aqueous ethanol (7.0 mL H_2O/12.0 mL EtOH) and stirred at 23 °C for 10 min. Next, TEOS (0.4 mL) was quickly added to the mixture and stirred 5 h, yielding monodisperse silica nanoparticles. For amine functionalization, APTMS (0.5 mL) was then added to the stirred silica-particle solution. Vigorous stirring of the solution was continued

overnight for 12 h, and then the solution was refluxed 1 h to ensure complete amine functionalization. To purify the silica particles, the solution was cooled to rt, centrifuged at 3000 rpm for 1 h and redispersed in 50 mL of ethanol. The cleansing cycle was repeated two times to ensure the purity of the APTMS-functionalized silica nanoparticles. Briefly, THPC-mNP seeds were assembled onto the silica cores by mixing 45 mL of the THPC-mNP seeds with the amine-functionalized silica cores (0.25 mL) with gentle shaking. The final mixed solutions were allowed to set 4 h, 2 h, and 1 h for the attachment of the THPC-AgNPs, THPC-PtNPs, and THPC-PdNPs seeds, respectively.

Growth of SiO_2-core metal nanoshells[7]

For producing the metal nanoshells, the appropriate reducible metal salt solution was first prepared. For silver nanoshells, the growth solution was produced by adding silver nitrate (0.002 g) to 50 mL of water. For platinum nanoshells, this was accomplished by adding 0.5 mL of 1 wt% K_2PtCl_4 to a solution of potassium carbonate (0.008 g in 34 mL of water), followed by vigorous stirring. For palladium nanoshells, a 0.5 mM solution of palladium chloride was prepared by dissolving 0.018 g of $PdCl_2$ in a mixture of 196 mL of water and 4 mL of a 50 mM HCl solution. The seeded growth of the metal nanoshells was initiated by first stirring 4 mL of the appropriate metal salt solution with varying amounts of THPC-mNP seeded silica nanoparticles (0.1 to 1.0 mL) in a 25 mL beaker for 5 min. It should be noted that adding more silica core particles to a set amount of metal salt solution decreases the shell thickness. Next, the desired metal shell was formed by the reduction of the corresponding metal salt using an appropriate reducing agent. Silver nanoshells were formed by simultaneously adding 50 mL of formaldehyde and 50 mL of ammonium hydroxide. Platinum nanoshells were formed by simply adding 50 mL of formaldehyde, and palladium shells were similarly formed using 0.3 mL of L-ascorbic acid (100 mM). To ensure complete shell growth, the reaction mixtures were vigorously stirred for 5 min. The metal nanoshells were then centrifuged at 2500 rpm for 15 min and redispersed in water, with no signs of aggregation.

Galvanic replacement of Pd with K-Gold[8]

Au nanocages were synthesized by galvanic replacement of Pd with Au. In a standard procedure, 6 mL of Pd nanocube(NC) solution, 300 μL of KI (from a 5 mM KI solution), and 50 mg of cetyltrimethyl ammonium bromide(CTAB) were added to a 40 mL vial. This mixture was heated to 50 °C in an oil bath with constant stirring at 400 rpm and kept at that temperature for 30 min. A 4 mL aliquot of K-gold solution was then added to the flask, the temperature was raised to 80 °C, and this temperature was maintained for 1.5 h. The resulting solution was then centrifuged at 5000 rpm, the supernatant was decanted, and the particles were redispersed in Millipore water. This procedure was repeated two times with the as-synthesized Pd@Au nanocages being redispersed in 6 mL of Millipore water. The amount of added KI and K-gold influences the course of the galvanic replacement reaction. Four representative samples of the Pd@Au nanocages (4 stages) were synthesized to illustrate the process of nanocage growth during the galvanic reaction. Also, an Au nanoframe was prepared by expanding the size of the facial openings of the nanocage as compared to that of the third-stage nanocage (Pd@Au). Separately, a Pd@Au nanoparticle having a spherical shape was synthesized using relatively large amounts of KI and K-gold.

Results and Discussion

Our research involved the synthesis of the GS-NS@SiO_2@ZIS core-shell particles and their photocatalytic hydrogen production. After preparing three sizes of GS-NSs with LSPR maxima centered at 500, 700, and 900 nm, coating the GS-NSs with a shell of silica (SiO_2) having two different thicknesses, 17 nm and 42 nm, surface modification, coated with the photocatalyst, zinc indium sulfide ($ZnIn_2S_4$; ZIS), we evaluated the photocatalytic water-splitting activities of these composites and compared the activities to that of undoped ZIS samples. Nanocomposites with a 17 nm interlaying silica shell surpassed those with no shell (i.e., a 2.6 times faster rate of H_2 production), but increasing the silica shell thickness to 42 nm had a detrimental effect on the photocatalytic activity, see Figure 1. These results indicate that the enhancements afforded by the GS-NSs@SiO_2 particles probably originate from improved charge transfer between the GS-NSs and the ZIS matrix via resonant energy transfer (RET) and local electromagnetic field enhancement (LEMF) mechanisms as shown in Scheme 1.[1]

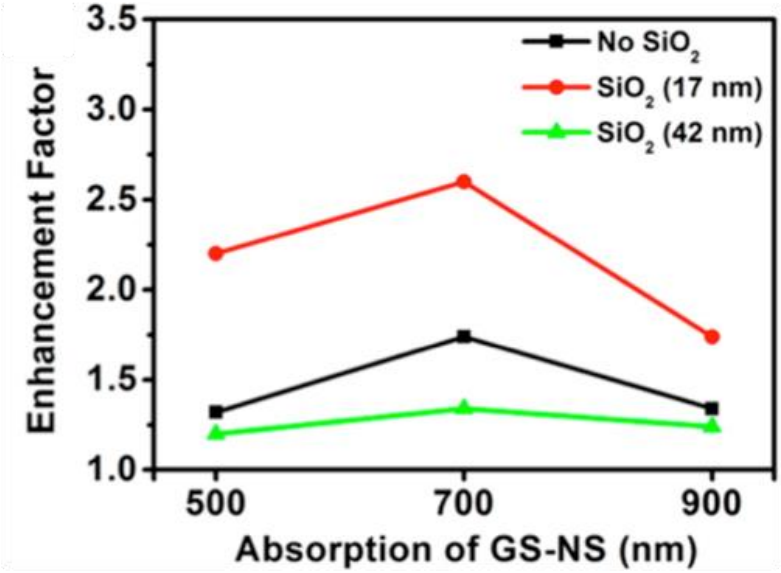

Figure 1. Enhancement in photocatalytic activities of GS-NS@SiO_2@ZIS samples with various silica coatings and selected GS-NSs absorption maxima. Reprinted with permission from reference 1 (Copyright 2016 American Chemical Society)

The lifetime of electron observed by time-resolved photoluminescence (TRPL).

To explore the charge-carrier dynamics, time-resolved photoluminescence (TRPL) was used to retrieve the lifetime of excited electrons in the conduction band. Figure 2(a) left shows the traditional TRPL setup that only one pulse laser was used. Coupled with time-correlated single photon counting (TCSPC), the charge carrier dynamics in the nanosecond regime associated with ZIS semiconductor can be studied. Here, 375 nm pulse laser was used to excite the valence electrons within ZIS matrix. Note that the energy band gap of ZIS is ~2.25 eV, which corresponds to an absorption at 550 nm. However, three types of GS-NS with LSPR maxima centered at 500, 700, and 900 nm covered with ZIS photocatalyst were used. One laser source cannot excite both the LSPR of GS-NS and electrons associated with ZIS at the same time. Thus, one additional light source was installed as the background light to excite the LSPR of the GS-

Scheme 1. Illustration of the Energy Transfer Mechanisms in ZIS Composites Doped with Silica-Coated GS-NSs. Adapted with permission from reference 1 (Copyright 2016 American Chemical Society).

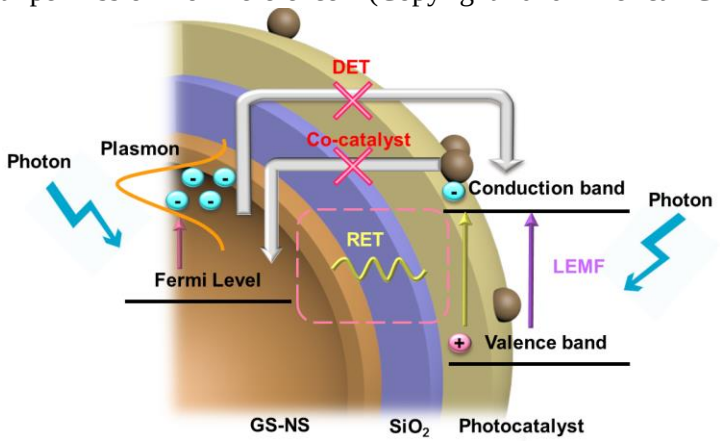

NSs. Here, continuous wave (CW) was used to denote the background illumination, in which a monochromatic light source was utilized (Figure 2(a) right). The photoluminescence was monitored continuously with time for each sample.

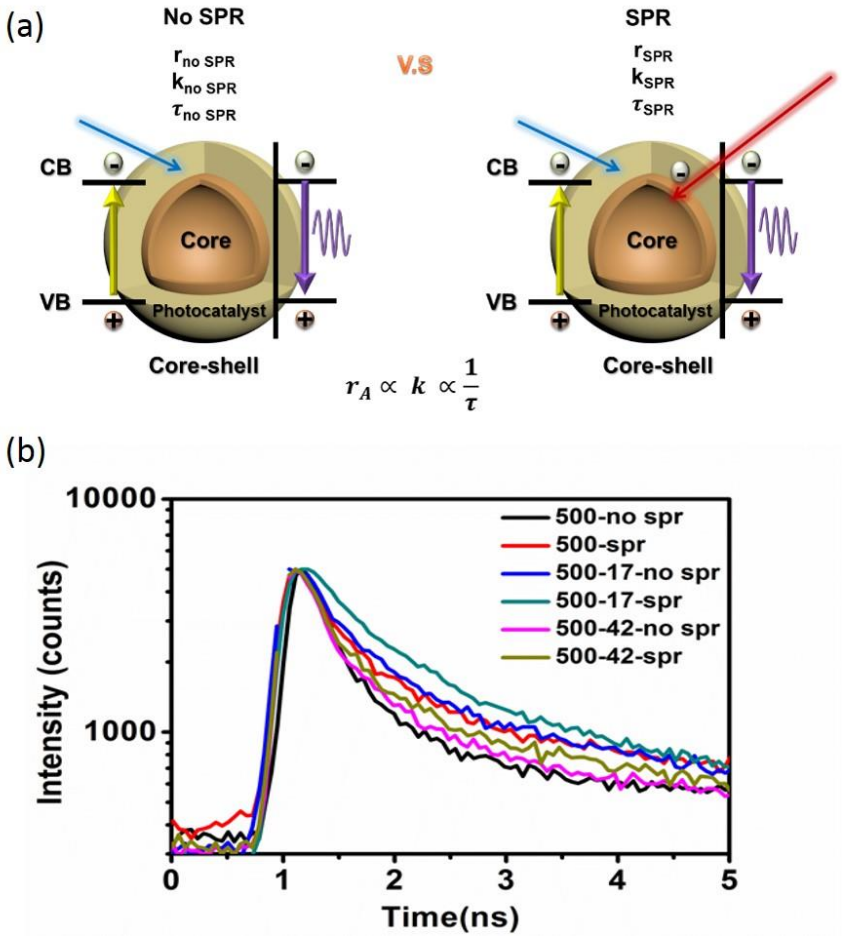

Figure 2. Time-resolved photoluminescence experiment (a) single pulse laser excitation (left) and single pulse laser excitation with continuous-wave light excitation (right). (b) PL intensity decay spectra.

The PL decay spectra are highly dependent on the lifetime of charge carriers, and assumed to be the first-order reaction kinetics (Figure 2(b)). The reaction rate and lifetime of charge carriers can be derived by fitting the data to the first-order reaction kinetics:

$$-r_{A^*} = -\frac{dC_{A^*}}{dt} = kC_{A^*}, r_{A^*} \propto k$$

$$ln\frac{C_{A^*}}{C_o} = -kt$$

$$\rightarrow C_{A^*} = C_o \cdot e^{-kt} \qquad k \propto \frac{1}{\tau}$$

$$\rightarrow r_A \propto k \propto \frac{1}{\tau}$$

The increase of charge carriers can be further derived by comparing the reaction rate with and without LSPR excitation through the following equation:

$$\text{Increase of charge carriers} = \frac{r_{no\ SPR} - r_{SPR}}{r_{no\ SPR}} = \frac{k_{no\ SPR} - k_{SPR}}{k_{no\ SPR}} = \frac{\frac{1}{\tau_{no\ SPR}} - \frac{1}{\tau_{SPR}}}{\frac{1}{\tau_{no\ SPR}}}$$

Finally, the data are shown in The effects of ZIS precursor concentration and the solid content of the SiO_2 particles were systematically studied. First, we compared the difference in the ZIS coating both with and without MPS surface modification. ***Figure 3*** shows TEM images of

Table 1. Although the CW light intensities of three excitation wavelengths were different, these TRPL data still can provide important information, such as the role of the SiO_2 thickness. From the hydrogen production experiment,[1,4] the interlayer of dielectric silica (SiO_2) between the GS-NSs and the ZIS photocatalyst is one of the key parameters to enhance the production of hydrogen and selectively terminate charge-transfer pathways to distinguish the charge-transfer mechanisms. The direct transfer of hot electrons from the GS-NSs to the ZIS photocatalyst was blocked by this layer. Of the 10 particle samples examined in this study, the most increase charge carriers was observed for GS-NSs having a SiO_2 interlayer thickness of~17 nm. However, for the GS-NS-containing particles with no SiO_2 interlayer, the charge carrier lies between that of the thin (~17 nm) and thick (~42 nm) SiO_2 interlayers. The reduced enhancement compared to the GS-NS(n)@SiO_2(17)@ZIS particles can be attributed to the absence of a dielectric interlayer whose blocking ability prevents the photoexcited electrons from transferring back to the GS-NS. Separately, the thicker shell reduces the contribution from the electric field effect upon the surrounding ZIS matrix. This observation agreed well with the TRPL data shown in Table 1. Our next step is to investigate further the direct electron transfer between photocatalyst and GS-NS without the SiO_2 interlayer. The results can shed light on the understanding the behavior of hot electron injection from the plasmonic nanoparticles directly into the semiconductor.

Thickness control of ZIS coating on the SiO_2 surface.

Our first generation GS-NS@SiO_2@ZIS exhibited promise for enhanced hydrogen production, due to the existence of plasmonic GS-NS.[1,4] However, a better control over the thickness of ZIS shell enables us to optimize further the sunlight absorption and photo-generated electron-hole

separation. In this study, SiO_2 particles were synthesized first with a similar size of the GS-NS@SiO_2 to mimic the surface chemistry. We used 3-mercaptopropyltrimethoxysilane (MPS) to modify the surface of the SiO_2 particles. The effects of ZIS precursor concentration and the solid content of the SiO_2 particles were systematically studied. First, we compared the difference in the ZIS coating both with and without MPS surface modification. ***Figure 3*** shows TEM images of

Table 1. Factors that Affect the Charge Carriers

CW light intensity (μW)	Sample	τ (ns)		Increase of charge carriers
		No SPR	SPR	
1.670	500-no	3.922	4.373	10.52%
	500-17	3.738	4.484	16.64%
	500-42	4.173	4.220	2.40%
0.779	700-no	3.326	3.466	4.04%
	700-17	3.559	3.910	8.98%
	700-42	3.181	3.212	0.97%
1.890	900-no	3.746	3.939	4.90%
	900-17	3.934	4.250	7.44%
	900-42	3.696	3.749	1.41%

the morphologies of the SiO_2@ZIS core-shell particles with (***Figure 3***(a)) and without (***Figure 3***(b)) the MPS surface modification. The figures show aggregation of ZIS on the SiO_2 without surface modification, but more homogeneous coverage on the SiO_2 with surface modification. Preferential adsorption of ZIS precursors onto the thiol functional group is evident from these TEM images. MPS modification will be applied to all of the SiO_2 particles in the following experiments.

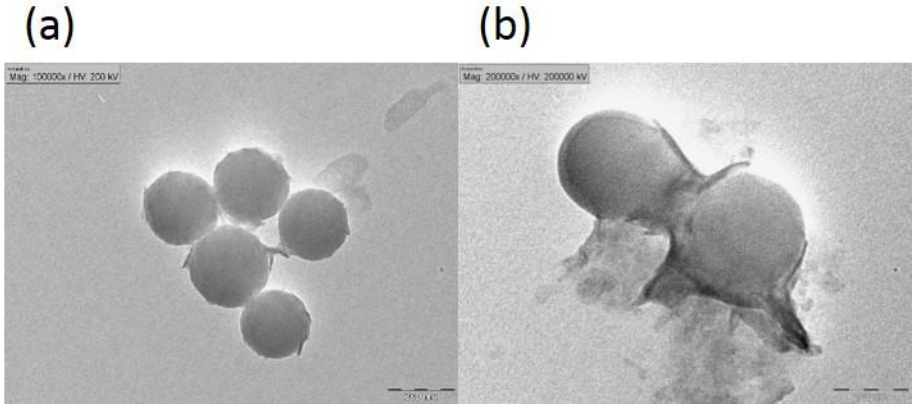

Figure 3. TEM images of aggregation of ZIS on the silica (a) with (b) without modification.

Next, we examined the influence of the ZIS precursor concentration. The concentration of ZIS precursor was increased from 5×10^{-5} to 5×10^{-4} M. As seen in ***Figure 4***(a), ZIS nucleated randomly on the SiO_2 surface and in the solution at the higher precursor concentration, creating sheet-like ZIS structures extending into the solution, rather than homogeneously growing on the

SiO_2 surface. In this microwave-assisted hydrothermal process, H_2S gas was generated during the reaction. A higher amount of ZIS precursor leads to higher pressure due to evolved gas, giving rise to a higher nucleation rate. We then examined the influence of the solid content of SiO_2 particles at a lower ZIS precursor concentration. Due to the lower solid content of the received GS-NSs, we decreased the concentration of SiO_2 particles to simulate the real situation. We observed that, with a decrease in the number density of SiO_2 particles, the heterogeneous nucleation sites also decrease (see ***Figure 4***(b)). Less nucleation density leads to aggregates of ZIS. In summary, uniform ZIS coatings on SiO_2 particles were obtained using lower concentration ZIS precursors and a higher SiO_2 solid content.

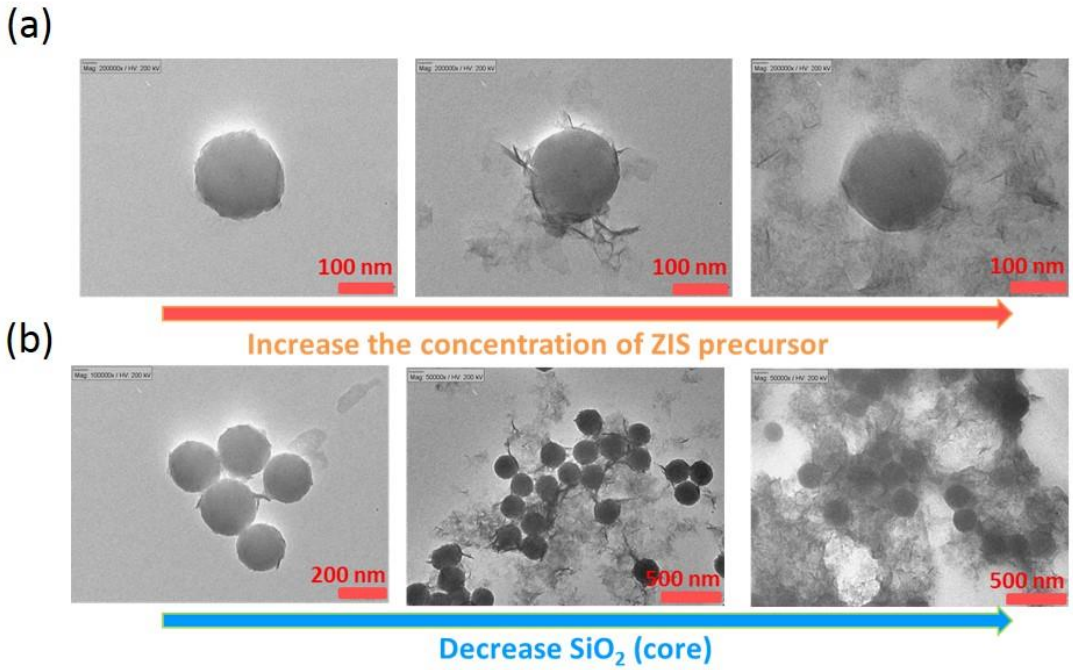

Figure 4. The effect of (a) concentration of ZIS precursor (b) silica content to the surface.

To this end, we have obtained a reprodicible procedure of preparing uniform ZIS coatings on SiO_2 particles. These parameters were used to synthesize various thicknesses of ZIS shell in a controlled fashion. First, the crystal structures of SiO_2@ZIS core-shell particles were examined using XRD. The pattern shows the diffraction peaks of ZIS, bare SiO_2, and the core-shell particle (

Figure 5(a)). The high-resolution TEM image of the core-shell particle shows the deposition of ZIS. The images below demonstrate a fringe spacing corresponding to the (102) plane of the hexagonal phase ZIS (

Figure 5(b)).

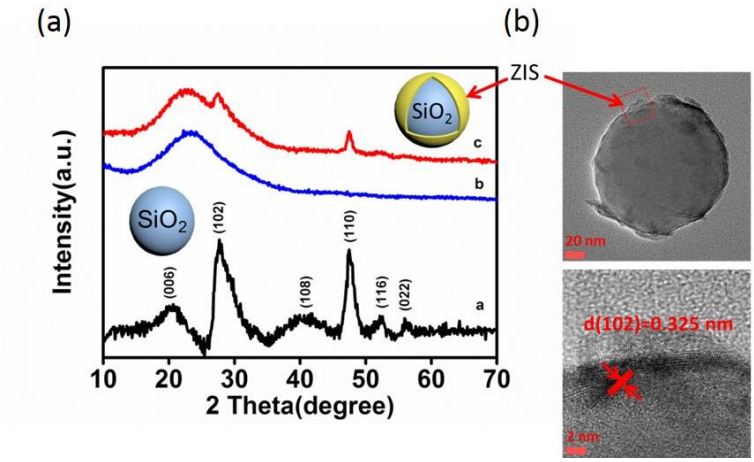

Figure 5. (a) XRD patterns of a. bare ZIS, b. bare SiO_2 and c. SiO_2@ZIS, and (b) TEM images of SiO_2@ZIS.

Secondly, the thickness of ZIS shell increases with an increase in reaction cycles. ***Figure 6*** shows the TEM images and corresponding increase in thickness of ZIS after each growth cycle. The diameters of SiO_2@ZIS core-shell particles were determined using dynamic light scattering (DLS) and directly from TEM images. Both data show similar results, with slightly larger particle sizes from the DLS measurements, due to the larger hydrodynamic radius. As seen in ***Table 2***, each deposition cycle increased the thickness of the ZIS shell by an average of ~9 nm.

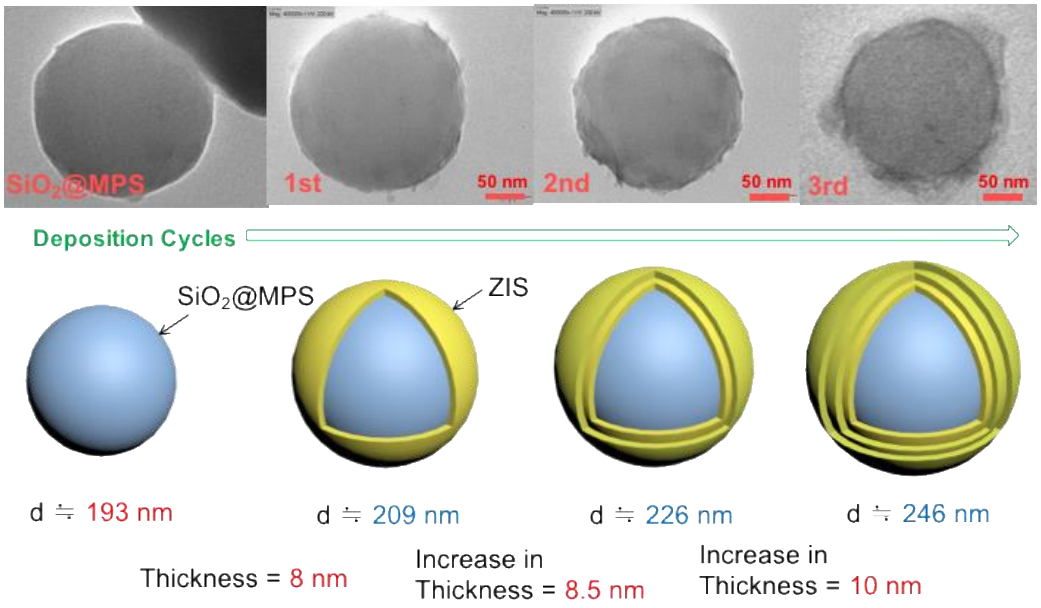

Figure 6. TEM images of SiO_2@ZIS particles with different ZIS deposition cycles.

Table 2. Average Diameter of SiO_2@ZIS Particles Determined Using DLS and TEM Images

	SiO_2	SiO_2@MPS	1st	2nd	3rd	4th
Average Diameter	182 ± 38	197 ± 53	223 ± 49	237 ± 52	268 ± 51	284 ± 69

From DLS (nm)						
Average Diameter From TEM (nm)	180 ± 6	192 ± 6	208 ± 6	225 ± 8	245 ± 6	266 ± 8

Finally, absorption and hydrogen production experiments were performed. An enhancement of absorption with increasing deposition cycle was observed (Figure 7(a)). The enhancement can be attributed to a thicker ZIS shell that can absorb more solar energy. However, the hydrogen production rate exhibits a different trend (Figure 7(b)). The H_2 evolution rate was calculated based on the weight of the active ZIS material. The H_2 production rate of bare ZIS is the lowest, indicating the worst utilization of photocatalyst among the samples tested. SiO_2@ZIS with only 1 deposition cycle showed the highest H_2 evolution rate. The H_2 evolution rate then gradually decreased with increasing ZIS thickness. Photocatalytic H_2 production arises from the competition between absorption and photo-generated electron-hole recombination. The crystallinity of the SiO_2@ZIS is not as good as that of bare ZIS, leading to a higher electron-hole recombination. On the other hand, the electron and hole diffusion length within the ZIS shell cannot be found in the literature. Continuing studies will enable us to modify our synthesis process to enhance the crystallinity of the ZIS shell, as well as to determine the charge transfer parameters using light-intensity modulation techniques.

In this part of our research, the experimental findings demonstrate that the surface modification on SiO_2 surfaces promotes nucleation of ZIS, leading to a homogeneous coverage. Additionally, the thickness of the ZIS shell can be easily tuned using microwave-assisted hydrothermal synthesis. Our facile procedure paves the way to generate an even more complex structure, GS-NS@dielectric@photocatalyst, for optimizing the production of solar hydrogen.

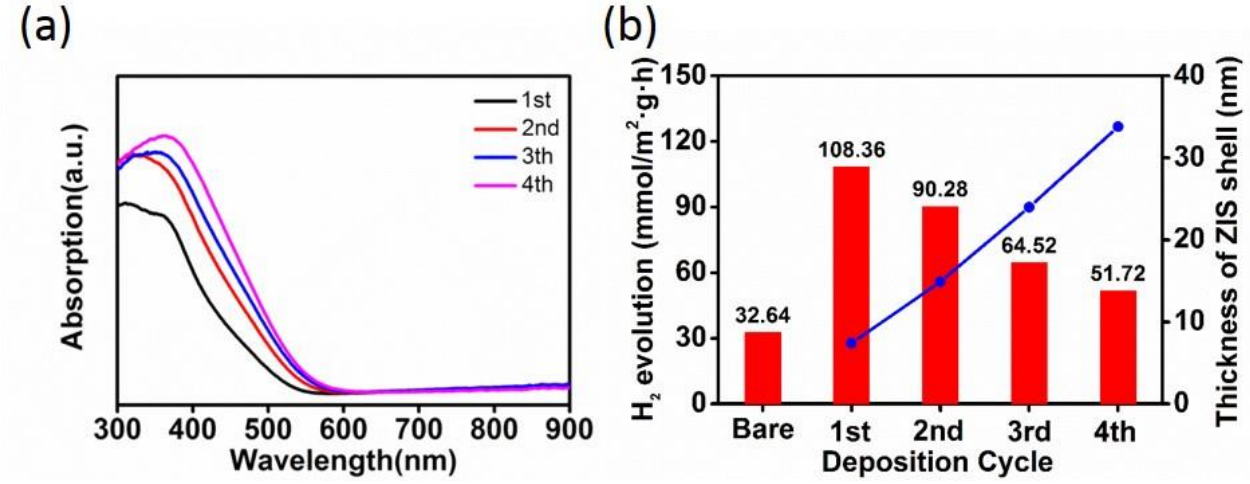

Figure 7. (a) Absorption (b) H_2 evolution of different deposition cycles of ZIS.

Coating of SnO_2 nanoshells.

We are also exploring the use of nanoshells coated with tin oxide rather (SnO_2) than silica (SiO_2). Tin-oxide (SnO_2) is an attractive material for coating plasmonic materials for photocatalytic reactions due to its excellent charge mobility. In addition, tin oxide-coated nanoparticles are more stable than silica coated ones over a wide range of pH conditions.[9] We anticipate that these properties will lead, not only to enhanced H_2 production, but also to photocatalytic devices with long-term stability. We are currently pursuing two kinds of SnO_2-coated GS-NSs. Our first approach starts with a silica-coated GS-NS core; subsequently, a thin layer of tin oxide is deposited on these particles. The formation of a SnO_2 layer simultaneously etches out the silica layer in a single step (Scheme 2). In this step, basic conditions (NaOH) facilitate the removal of the silica shell and assist with the SnO_2-coating process. Nanoshells generated from this method exhibit a yolk-shell type structure with a void space between the tin oxide shell and the GS-NS core. These new particles have been prepared at the university of Houston (see Figure 8) and shipped to National Central University in Taiwan for analysis of their photocatalytic activity as co-catalysts for hydrogen production.

Scheme 2. Strategy for the Synthesis of SnO_2-Coated Yolk-Shell Nanoparticles.

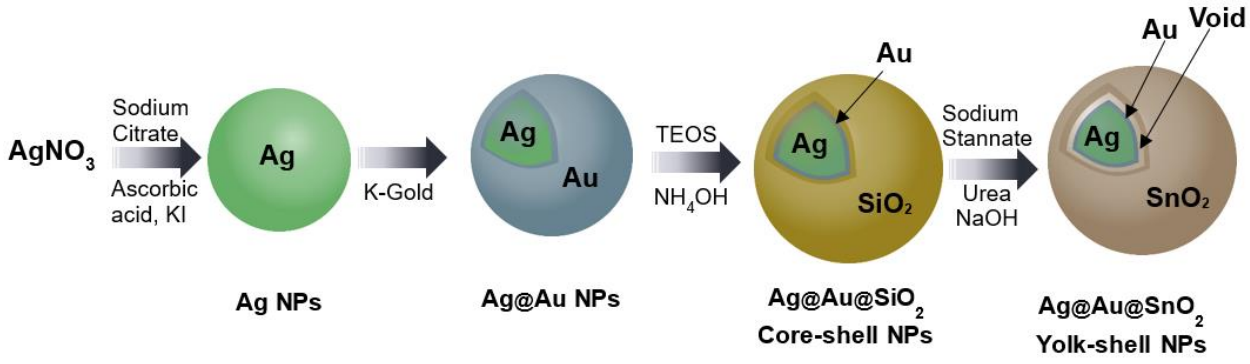

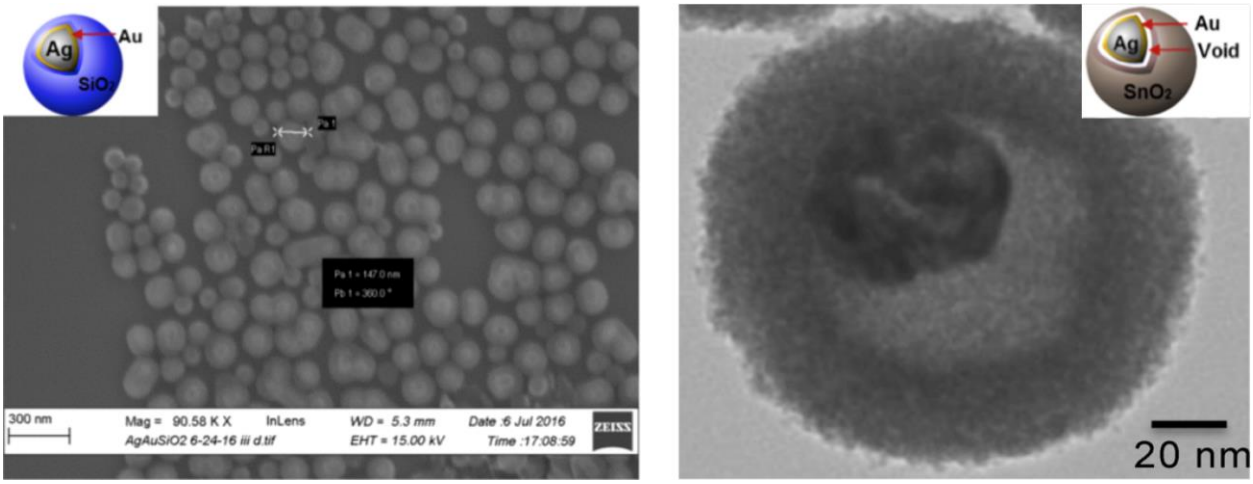

Figure 8. SiO_2-coated GS-NS particles (left) and SnO_2-coated yolk-shell GS-NSs (right).

The second approach involves the direct coating of a tin oxide layer on the GS-NSs to afford a core-shell structure (Scheme 3). These particles show a broad extinction in the near infrared that extends beyond 1000 nm (see Figure 9).

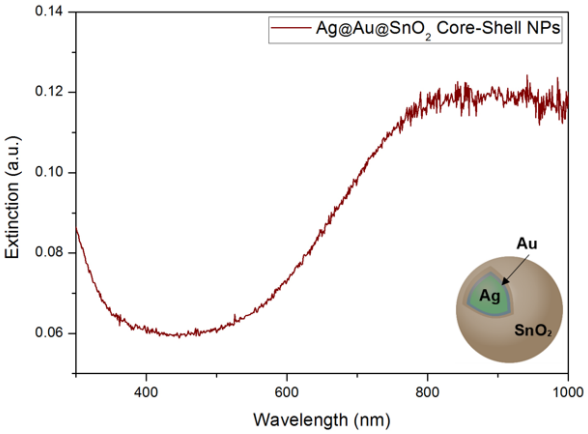

Figure 9. Extinction spectrum of SnO_2-coated GS-NSs.

Scheme 3. Synthesis of SnO_2-Coated GS-NSs.

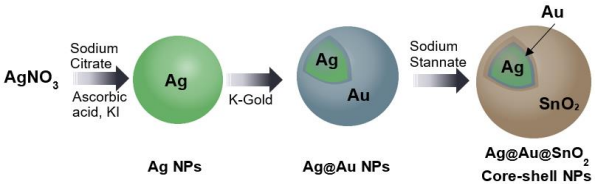

These two newly developed classes of tin oxide-coated nanoparticles will be used to fabricate a second generation of ZIS-based photocatalytic systems. Subsequently, their performance will be compared to the earlier mentioned first-generation ZIS photocatalysts (described above having silica shells). Such comparisons will further our understanding of the fundamental energy-transfer mechanisms occurring within these composite particles.

We are also developing methods to coat the GS-NSs with zinc- and antimony-doped SnO_2 (Scheme 4); examples of our recent syntheses of these new particles are shown in Figure 10. Doped oxide films, commonly called transparent conducting oxides (TCOs), have shown great promise in photoelectrochemical reactions. Synthetic routes for the preparation of these particles are currently being optimized, and their optical properties are being studied. Other possible dopants are also being considered for enhancing the properties of our composite system. In addition, we are seeking an alternative recipe for the synthesis of Ag nanoparticles that is more reproducible than our current one (and one that gives exclusively spherical particles).

Scheme 4. Strategy for Coating GS-NSs with Zn- and Sb-Doped SnO_2 (ZTO and ATO).

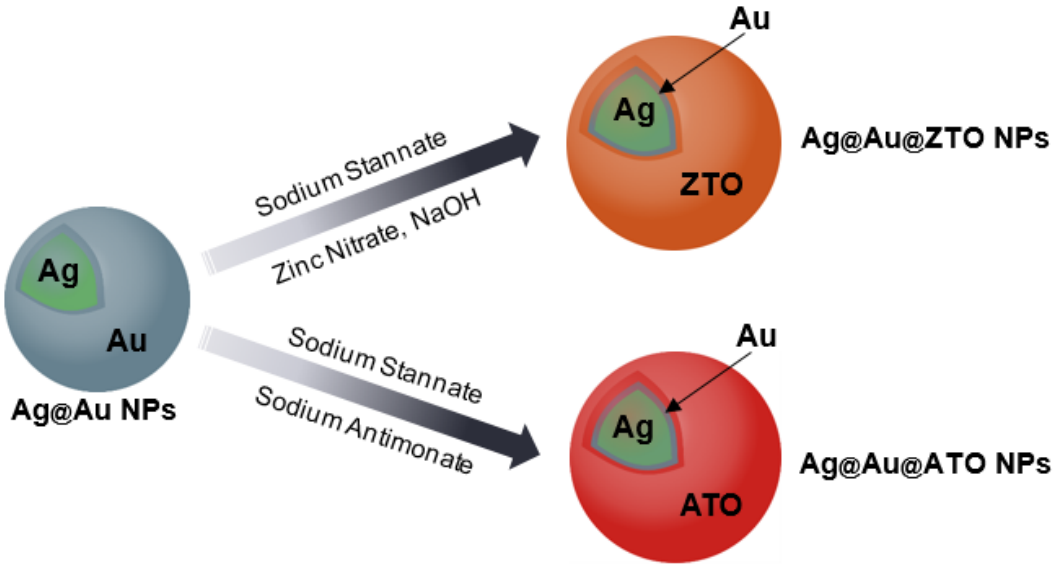

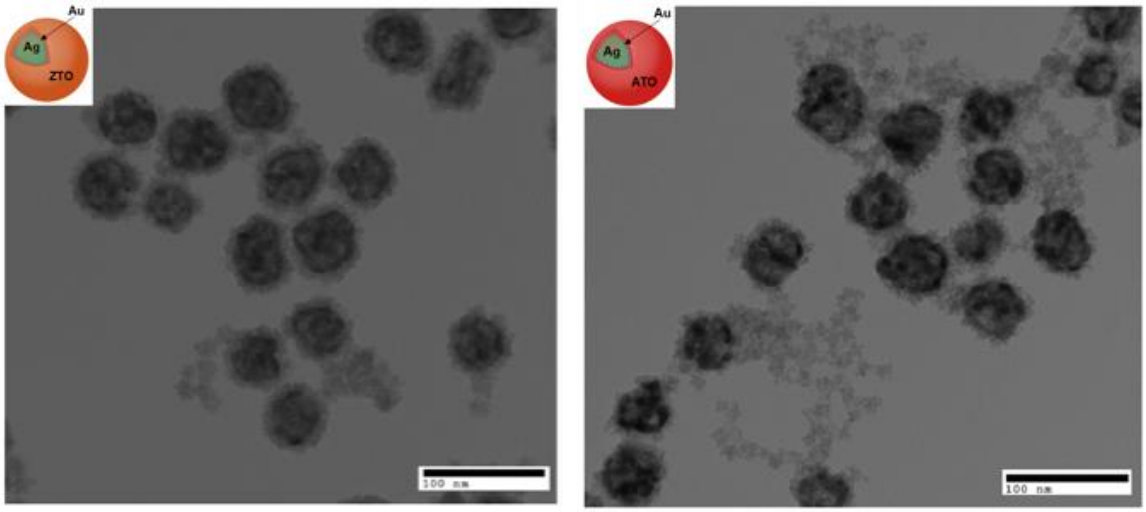

Figure 10. TEM images of GS-NSs core coated with ZTO (left) and ATO (right).

Metal seed nanoparticles.

As part of our ongoing efforts to improve the synthesis of metal nanoshells, we developed new routes for the preparation of silver, platinum, and palladium seed nanoparticles functionalized with tetrakis(hydroxymethyl)phosphonium chloride (THPC), and demonstrated their use in the synthesis of Ag, Pt, Pd, and Pt/Ag Nanoshells, see Scheme 5.[7] While the use of THPC-gold nanoparticles to seed metal nanoshells is well known, the process is time consuming and requires highly concentrated seeding solutions. Our THPC-mNPs were used to rapidly seed the growth of a variety of metal nanoshells, including the successful generation of highly uniform platinum and palladium nanoshells grown from their own seeds.

Scheme 5. Strategy for the Synthesis of Metal Nanoshells (Ag, Pt, and Pd) using THPC-Coated mNPs.

THPC: Tetrakis(hydroxyr
THPC-mNPs: Ag, Pt, a

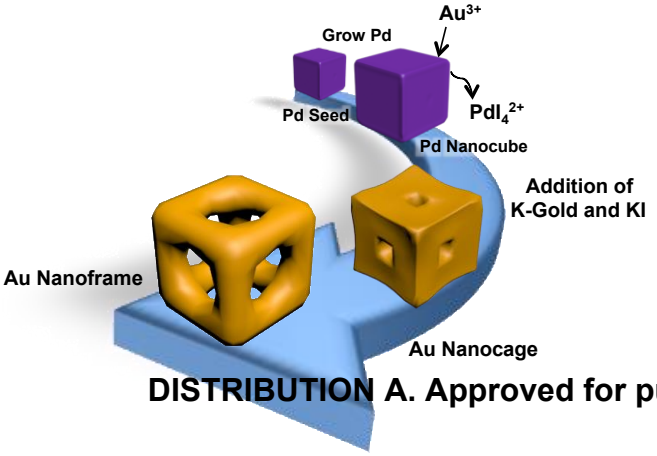

In addition to the GS-NS plasmonic-based systems, we explored the preparation of silver-free Au nanocages from cubic palladium templates (Scheme 6).[8] Pd nanocubes were subjected to galvanic replacement with Au^{3+} to produce Pd@Au nanocages having

tunabledimensions (i.e., edge length, gold layer thickness, and hollow pore size), which allowed selectable positioning of the optical extinction maxima from the visible to the near infrared (see Figure 11). These new nanocages circumvent the problems associated with previous Ag-derived gold alloy nanocages, which suffer from the toxicity of residual silver and the possible fragmentation of such alloyed nanostructures, thereby limiting their potential applications. In contrast, the present materials represent stable, nontoxic, tunable, hollow plasmonic nanostructures.

Photonic iron oxide nanoparticles (Fe3O4) as co-catalysts.

Separate studies are exploring the use of photonic iron oxide (Fe_3O_4) nanoparticles as co-catalysts in photocatalytic water splitting. We are in the process of synthesizing highly crystalline Fe_3O_4 nanospheres and nanocubes, and we are evaluating their visible to NIR absorptions to determine the influence of shape, size, and crystallinity on the corresponding optical properties. Our preliminary results indicate thus far that highly crystalline Fe_3O_4 nanoparticles with a spherical morphology show a broad optical absorption over the visible to NIR range with absorption maxima centered at 650 nm (see Figure 12a) or even longer wavelengths (see Figure 12b).

Scheme 6. Synthesis Strategy for Preparing Tunable Au Nanocages. Adapted from reference 8.

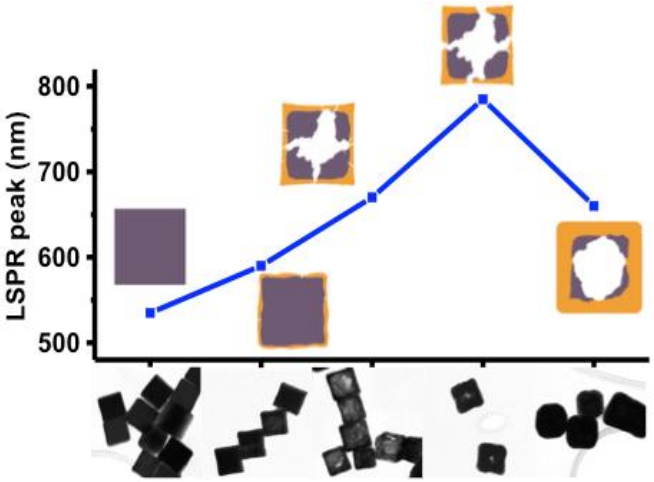

Figure 11. Morphological changes of Pd@Au nanocages at different stages of galvanic replacement reaction and their corresponding LSPR peak positions. Adapted from reference 8.

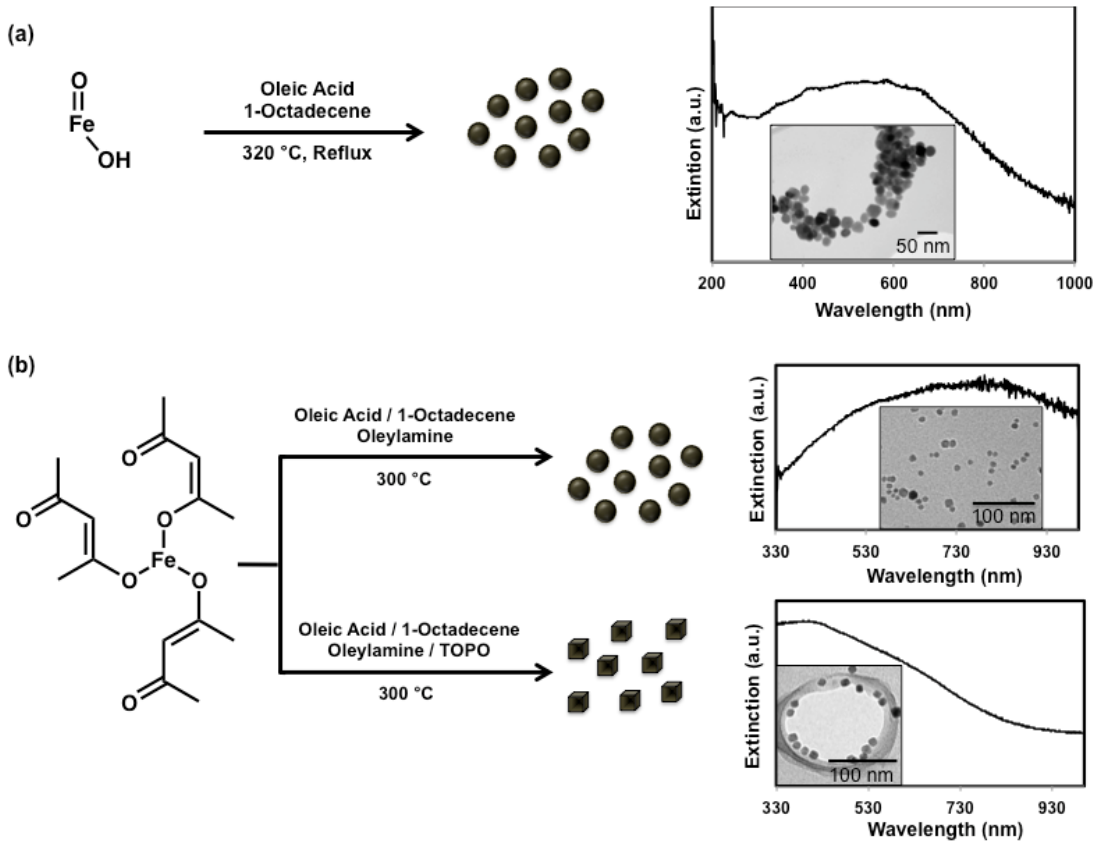

Figure 12. Synthetic methods, extinction spectra, and TEM images of spherical and cubic Fe_3O_4 nanoparticles prepared via (a) thermal decomposition and (b) a solvothermal process.

List of Publications and Significant Collaborations

Publications

- Lin, P.-C.; Wang, P.-Y.; Li, Y.-Y.; Hua, C. C.; Lee, T.-C., Enhanced Photocatalytic Hydrogen Production over In-rich (Ag-In-Zn)S Particles. *Int. J. Hydrogen Energy* **2013**, *38*, 8254-8262. (AFOSR/AOARD: FA2386-11-1-4081)
- Lee, F.-Y.; Yang, K.-Y.; Wang, Y.-C.; Li, C.-H.; Lee, T. R.; Lee, T.-C., Electrochemical Properties of an $AgInS_2$ Photoanode Prepared Using Ultrasonic-assisted Chemical Bath Deposition. *RSC Adv.* **2014**, *4*, 35215-35223. (AFOSR/AOARD: FA2386-13-1-4032)

- Li, C.-H.; Jamison, A. C.; Rittikulsittichai, S.; Lee, T.-C.; Lee, T. R., In Situ Growth of Hollow Gold–Silver Nanoshells within Porous Silica Offers Tunable Plasmonic Extinctions and Enhanced Colloidal Stability. *ACS Appl. Mater. Interfaces* **2014**, *6*, 19943-19950. (AFOSR/AOARD: FA2386-13-1-4032)
- Zhao, F.; Zeng, J; Arnob, M. M. P.; Sun, P.; Qi, J.; Motwani, P.; Gheewala, M.; Li; Paterson, A.; Strych, U.; Raja, B.; Willson, R. C.; Wolfe, J. C.; Lee, T. R.; Shih, W.-C., Monolithic NPG Nanoparticles with Large Surface Area, Tunable Plasmonics, and High-Density Internal Hot-Spots. *Nanoscale* **2014**, *6*, 8199-8207. (AFOSR/AOARD: FA2386-13-1-4032)
- Li, C.-H.; Li, M.-C.; Jamison, A. C.; Liu, S.-P.; Lee, T. R.; Lee, T.-C., Plasmonically Enhanced Photocatalytic Hydrogen Production from Water: The Critical Role of Tunable Surface Plasmon Resonance from Gold-Silver Nanoshells. *ACS Appl. Mater. Interfaces* **2016**, *8*, 9152-9161. (AFOSR/AOARD: FA2386-14-1-4074 and FA2386-15-1-4101)
- Bryan, W. W.; Jamison, A. C.; Chinwangso, P.; Rittikulsittichai, S.;Lee, T.–C.; Lee, T. R., Preparation of THPC-Generated Silver, Platinum, and Palladium Nanoparticles and Their Use in the Synthesis of Ag, Pt, Pd, and Pt/Ag Nanoshells. *RSC Adv.* **2016**, *6*, 68150-68159. (AFOSR/AOARD: FA2386-15-1-4101)
- Shakiba, A.; Shah, S.; Jamison, A. C.; Rusakova, I.; Lee, T. -C.; Lee. T. R., Silver-Free Gold Nanocages with Near Infrared Extinctions. *ACS Omega*, **2016**, *1*, 456-463. (AFOSR/AOARD FA2386-15-1-4101 and DURIP FA9550-15-1-0374)
- Lin, P.-C.; Lee, T.-C., Correlation between Photocatalytic Activities and Band Positions of (M-In-Zn)S (M = Cu and/or Ag) Solid Solutions, In preparation. (AFOSR/AOARD: FA2386-11-1-4081)

Presentations

- T.-C. Lee (2011, Sep). 14th Asian Chemical Congress 2011, Bangkok, Thailand.
- T.-C. Lee (2012, May). Invited talk: National Chiao Tung University, Hsinchu, Taiwan.
- T. R. Lee (2012, June). Invited talk: Functional Molecules and Materials Symposium; Walailak University; Nakhon Si Thammarat, Thailand.
- P.-C. Lin and T.-C. Lee (2012, Jul). International Conference of Young Research on Advanced Materials, Singapore.
- T.-C. Lee (2013, Apr.). Invited talk: Chang Gung University, Taoyuan, Taiwan.
- T. R. Lee (2013, July). Invited talk: Indo-US Symposium on Molecular Materials; Bangalore, India.
- Y.-K. Kuo, K.-Y. Yang, and T.-C. Lee (2014, Aug). The 15th IUMRS-International Conference in Asia, Fukuoka, Japan.
- T.-C. Lee and T. R. Lee (2014, Sep). Air Force Research Laboratory, Dayton, Ohio, USA.
- M.-C. Li, P.-C. Lin, T. R. Lee, and T.-C. Lee (2014, Oct). VASSCAA-7, Hsinchu, Taiwan.
- C.-H. Li, T.-C. Lee, and T. R. Lee (2014, Oct). BASF-UH Joint Symposium, Univ. of Houston, Houston, TX, USA.
- T.-C. Lee (2014, Dec.). Invited talk: National Chung Hsing University, Taichung, Taiwan.

- C.-H. Li, T.-C. Lee, and T. R. Lee (2015, Mar). 249th ACS National Meeting & Exposition, Denver, CO, USA.
- T.-C. Lee (2015, Jun.). Invited talk: National Synchrotron Radiation Research Center, Hsinchu, Taiwan.
- T. R. Lee (2015, Oct.). Invited talk: Sogang University; Seoul, South Korea.
- T. R. Lee (2016, May). Keynote Speaker: Research First Look Symposium; Houston, Texas.
- T. R. Lee (2016, May). Invited talk: University of California at Davis; Davis, California.
- T. R. Lee (2016, Jun.). Invited talk: University of California at Merced; Merced, California.

Interaction/Collaboration with AFRL, DoD, Industry

- T.-C. Lee and T. R. Lee (Sep. 10, 2014). Visited United States Air Force Research Laboratory in Dayton, OH.
- T. R. Lee (Aug. 17-18, 2015). Hosted the visit of Dr. Kenneth Caster at the University of Houston, Houston, TX.
- T. R. Lee (Oct. 2, 2015). Met with Dr. Ajit Roy at the University of Houston, Houston, TX.
- T. R. Lee (Oct. 16, 2015). Hosted the visit of Dr. Christopher Bunker, University of Houston, Houston, TX.
- T. R. Lee (Oct. 17, 2015). Hosted Dr. Christopher Bunker and Mr. Donald Minus at the *Houston Energy Day Festival http://energydayfestival.org/*, Houston, TX. *T. R. Lee (Apr. 15, 2016).*
- T. R. Lee (Apr. 15, 2016). *Held preliminary discussions with Dr. Dennis Butcher about starting a new initiative involving the University of Houston, AFOSR, and CONACYT (Mexico's funding agency).*

Team Collaboration Synergy Highlights

- Student exchange, Pei-Ying Wang (Jun. 2012) visited UH
- Student exchange, Po-Chang Lin (Jul. 2013) visited UH
- Student exchange, Henry Li (May 2014) visited NCU
- PI visit, T. Randall Lee (May 2014) visited NCU
- PI visit, Tai-Chou Lee (Sep. 2014) visited UH
- Student exchange, Henry Li (Sep. 2015) visited NCU
- Student exchange, Si-Ping Liu (Apr. 2016) visited UH
- PI visit, T. Randall Lee (Oct. 2016) visited NCU

References

1. C.-H. Li; M.-C. Li; S.-P. Liu; A. C. Jamison; D. Lee; T. R. Lee; T.-C. Lee, *ACS Appl. Mater. Interfaces* **2016**, *8*, 9152-9161. Support from FA2386-15-1-4101 acknowledged.

2. S. Ren; B. Wang.; H. Zhang; P. Ding; Q. Wang, *ACS Appl. Mater. Interfaces* **2015,** *7*, 4066-4074.

3. C.-S. Chang; L. J. Rothberg, *Chem. Mater.* **2015**, *27*, 3211-3215.

4. S. K. Cushing; J. Li; F. Meng; T. R. Senty; S. Suri; M. Zhi; M. Li; A. D. Bristow; N. Wu, *J. Am. Chem. Soc.* **2012**, *134*, 15033-15041.

5. V. Vongsavat; B. M. Vittur; W. W. Bryan; J.-H. Kim; T. R. Lee, *ACS Appl. Mater. Interfaces* **2011**, *3*, 3616-3624.

6. Stober, W.; Fink, A.; Bohn, E. Controlled Growth of Monodisperse Silica Spheres in the Micron Size Range. *J. Colloid Interface Sci.* **1968**, *26*, 62−69.

7. W. W. Bryan; A. C. Jamison; P. Chinwangso; S. Rittikulsittichai; T.-C. Lee; T. R. Lee, *RSC Advances* **2016**, *6*, 68150-68159. Support from FA2386-15-1-4101 acknowledged.

8. A. Shakiba; S. Shah; A. C. Jamison; I. Rusakova; T.-C. Lee; T. R. Lee, *ACS Omega* **2016**, *1*, 456-463. Support from FA2386-15-1-4101 acknowledged.

9. S. H. Lee; I. Rusakova; D. M. Hoffman; A. J. Jacobson; T. R. Lee, *ACS Appl. Mater. Interfaces* **2013**, *5*, 2479-2484.